Differential Dynamics at Glycosidic Linkages of an Oligosaccharide as Revealed by 13C NMR Spin Relaxation and Stochastic Modeling

Differential Dynamics at Glycosidic Linkages of an Oligosaccharide as Revealed by ^{13}C NMR Spin Relaxation and Stochastic Modeling

Mirco Zerbetto[a], Thibault Angles d'Ortoli[b], Antonino Polimeno[a,*], and Göran Widmalm[b,*]

[a] Dipartimento di Scienze Chimiche, Università degli Studi di Padova, Padova 35131, Italy

[b] Department of Organic Chemistry, Arrhenius Laboratory, Stockholm University, S-106 91 Stockholm, Sweden

Corresponding authors. *E-mail: antonino.polimeno@unipd.it and goran.widmalm@su.se

Abstract

Among biomolecules, carbohydrates are unique in that not only can linkages be formed through different positions but the structures may also be branched. The trisaccharide β-D-Glc*p*-(1→3)[β-D-Glc*p*-(1→2)]-α-D-Man*p*-OMe represents a model of a branched vicinally disubstituted structure. A ^{13}C site-specific isotopologue with labeling in each of the two terminal glucosyl residues enabled acquisition of high-quality ^{13}C NMR relaxation parameters T_1, T_2 and heteronuclear NOE, with standard deviations of ≤ 0.5%. For interpretation of the experimental NMR data a diffusive chain model was used in which the dynamics of the glycosidic linkages is coupled to the global reorientation motion of the trisaccharide. Brownian dynamics simulations relying on the potential of mean force at the glycosidic linkages were employed to evaluate spectral densities of the spin probes. Calculated NMR relaxation parameters showed very good agreement with experimental data, deviating < 3%. The resulting dynamics is described by correlation times of 196 ps and 174 ps for the β-(1→2)- and β-(1→3)-linked glucosyl residues, respectively, i.e., different and linkage dependent. Notably, the devised computational protocol was performed without any fitting of parameters.

Introduction

Biomolecules such as nucleic acids and proteins are formed as linear sequences of their building blocks whereas carbohydrates, also known as glycans in biological systems, are linked not only by sequential addition of residues but may be highly branched thereby already on the connectivity level of entities will be highly complex.[1] The detailed three-dimensional structure of these biomolecules is commonly elucidated by means of X-ray crystallography or NMR spectroscopy,[2] but cryo-electron microscopy[3] also contributes, in particular, for large structures. Dynamics, on the other hand, is typically studied by fluorescence depolarization[4] or NMR spectroscopy[5] depending on the probe available within the molecule.

Carbohydrate structures may be built in many different forms having the D or L absolute configuration, with furanose and pyranose ring forms commonly observed, either having the α- or β-anomeric configuration and as branched in one or more positions, a feature seen in oligosaccharides linked to proteins as glycoconjugates[6] and in lipopolysaccharides (LPS) with short chains substituting a core region in the amphiphilic LPS molecule or as long O-antigen polysaccharides connected to the core structure.[7] The polysaccharide structures may be branched and very large on the order of MDa as observed for capsular polysaccharides and exopolysaccharides.[8] The branching pattern of a sugar residue may take several forms some of which have sugars linked to it by non-adjacent residues and the conformational space of the oligosaccharide can be anticipated to be described by conformational dynamics at each of the glycosidic linkages.[9] However, depending on the absolute configuration, the anomeric configuration or the sugar residues per se that vicinally di- or multisubstitute another sugar entity significantly altered conformational preferences may result[10] as well as the dynamics present.

The trisaccharide β-D-Glc*p*-(1→3)[β-D-Glc*p*-(1→2)]-α-D-Man*p*-OMe[11] (GGM) (Figure 1) represents a model for branched structures, in which the glucosyl residues vicinally substitute positions 2 and 3 of the mannosyl residue. Its conformational preferences and dynamics in solution have previously been studied by ^{1}H,^{1}H-NOE NMR methodology[12] and ^{13}C NMR spin relaxation experiments at ^{13}C natural abundance.[13] Recently, we showed that excellent NMR spin relaxation data were possible to obtain for a single site-selectively ^{13}C-labeled disaccharide where the relaxation parameters were possible to model in very good agreement (average error < 2%) using a stochastic approach. In particular, we employed the diffusive chain model (DCM),[14] which proved very effective to predict NMR relaxation data of 'linear' oligosaccharides, with two, three, and five sugar units.[15,16,17] The method is based on the description of the internal degrees of freedom (dof) of a molecule in terms of bonds, bond angles and dihedral angles. The former two types of internal dof are considered fast and therefore not relevant to NMR-based investigations of molecular structure and dynamics. Among the remaining dof, a selection of the relevant dihedral angles is carried out,

based on the correlation times of the dihedral angles calculated from molecular dynamics simulations. The selected dihedral angles are then coupled to the global rotation of the molecule. The DCM has been applied to the study of NMR[15,16,17] and EPR[18,19] spectroscopy of small flexible molecules with parameters entering the model easily linked to the molecular geometry.

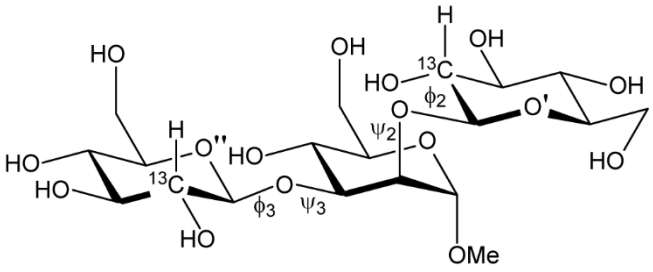

Figure 1. Schematic of the site-specifically carbon-13 labeled disaccharide β-D-[1''-^{13}C]Glc*p*-(1→3)[β-D-[1'-^{13}C]Glc*p*-(1→2)]-α-D-Man*p*-OMe with pertinent glycosidic torsion angles indicated by ϕ and ψ.

The conformational preferences of GGM were recently analyzed based, inter alia, on transglycosidic $^{3}J_{CC}$ using synthesized site-selectively ^{13}C-labeled forms of the trisaccharide, where one of these was a doubly site-selectively ^{13}C-labeled variant.[11] This labeling-pattern facilitates investigation of the dynamics of the two glucosyl residues under identical experimental conditions and we here report NMR spin relaxation data of the trisaccharide and subsequent analysis thereof using the DCM model based on Brownian dynamics simulations.

Material and Methods

General. In the trisaccharide β-D-Glc*p*-(1→3)[β-D-Glc*p*-(1→2)]-α-D-Man*p*-OMe (GGM)[20] the atoms in the terminal (1→2)-linked glucosyl residue are denoted by a prime, those in the terminal (1→3)-linked glucosyl residue are denoted by a double prime whereas those in the mannosyl residue linked to the *O*-methyl group are non-primed. The glycosidic torsion angles between the sugar residues are defined as follows: ϕ_2 = H1'-C1'-O2-C2, ψ_2 = C1'-O2-C2-H2, ϕ_3 = H1''-C1''-O3-C3, ψ_3 = C1''-O3-C3-H3. The synthesis of the site-specifically carbon-13 labeled disaccharide β-D-[2''-^{13}C]Glc*p*-(1→3)[β-D-[2'-^{13}C]Glc*p*-(1→2)]-α-D-Man*p*-OMe has been described[11] and the molecule is referred to as [$^{13}C_2$]-GGM.

NMR spectroscopy experiments. All NMR experiments were recorded on a sample of [$^{13}C_2$]-GGM in D_2O (13 mg in 0.5 mL, 50 mM) at 298.6 K where the temperature had been calibrated by a methanol-d_4 sample[21] prior to the start the experiments and processing of the acquired data was

carried out using TopSpin 3.1 (Bruker). ^{1}H and ^{13}C NMR chemical shifts of GGM in D_2O are known from literature.[20]

The ^{13}C NMR relaxation experiments were performed on a Bruker AVANCE III 700 MHz spectrometer (16.44 T) equipped with a 5 mm TCI Z-Gradient Cryoprobe and a Bruker AVANCE III 600 MHz spectrometer (14.09 T) equipped with a 5 mm BBO probe. The experiments were recorded with the carrier set in the region (70 – 75 ppm) near the ^{13}C-labeled resonances of [$^{13}C_2$]-GGM and inter-scan delays > 10 s. Longitudinal relaxation times (T_1) were measured with the fast inversion recovery experiment[22] using 14 different relaxation time delays ranging between 0.005 and 3.2 s in a shuffled manner for each experiment. Spectra were recorded with 32 scans, 16k data points and a spectral width of 190 ppm. An exponential window function of 5 Hz was applied prior Fourier transformation whereupon peak intensities were extracted. The relaxation times were then fitted based on the peak intensities and average values were calculated from 6 and 7 independent experiments, at the lower and higher magnetic field strengths, respectively. Transverse relaxation times (T_2) were measured using a Carr-Purcell-Meiboom-Gill (CPMG) pulse sequence.[23] The delays between ^{13}C refocusing pulses in the pulse trains were set to 0.25 and 0.50 ms, at 14.09 T and at 16.44 T, respectively, and the total length of the pulse-train was varied ten times in a shuffled manner for each experiment with a total pulse-train length from 20 to 300 ms. Spectra were recorded with 32 or 64 scans, using either 16k or 32k data points, and spectral widths of 100 or 120 ppm; an exponential window function of 5 Hz was applied prior Fourier transformation. The T_2 relaxation times were then calculated from 14 and 30 independent experiments, at the lower and higher magnetic field strengths, respectively. The NOE enhancements were calculated from the intensity ratios of a steady state NOE experiment with one long ^{1}H radiation time (5 s) and one short (1 ms). Spectra were recorded with either 256 or 512 scans, 64k data points and a spectral width of 190 ppm; an exponential window function of 3 Hz was applied prior Fourier transformation. Average NOE enhancement values were calculated from 6 and 7 experiments, at the lower and higher magnetic field strengths, respectively.

Diffusive chain model. Based on past experience on oligosaccharides,[15,16,17] we model the relevant dynamics of GGM in terms of a few, relevant, torsion angles coupled to the global rotational motion of the molecule. We call this set $\mathbf{Q}=(\mathbf{\Omega},\boldsymbol{\theta})$, where $\mathbf{\Omega}$ is the set of Euler angles providing the orientation of the molecule in the laboratory frame where the magnetic field is defined, and $\boldsymbol{\theta}=[\phi_2,\psi_2,\phi_3,\psi_3]$ is the array that collects the relevant torsion angles for the trisaccharide. The remaining coordinates of the molecule and the solvent ones are relegated to the role of the thermal bath to which the selected relevant coordinates are in thermodynamic equilibrium. The bath is described as a generator of fluctuation-dissipation over $\mathbf{Q}$ and provides a mean-field contribution to

the energetics on $\mathbf{Q}$. The dynamics of the relevant degrees of freedom is thus stochastic and in the high friction regime; the equation that governs the time evolution of the system is the Smoluchowski equation

$$\frac{\partial}{\partial t}P(\mathbf{Q},t) = -\hat{\Gamma}(\mathbf{Q})P(\mathbf{Q},t) = -\begin{bmatrix}\hat{\mathbf{M}}(\boldsymbol{\Omega}) \\ \partial/\partial\boldsymbol{\theta}\end{bmatrix}^{tr}\begin{bmatrix}\mathbf{D}_{RR} & \mathbf{D}_{RI} \\ \mathbf{D}_{RI}^{tr} & \mathbf{D}_{II}\end{bmatrix}P_{eq}(\mathbf{Q})\begin{bmatrix}\hat{\mathbf{M}}(\boldsymbol{\Omega}) \\ \partial/\partial\boldsymbol{\theta}\end{bmatrix}P_{eq}^{-1}(\mathbf{Q})P(\mathbf{Q},t) \qquad (1)$$

where $P(\mathbf{Q},t)$ is the probability density of finding the system in configuration $\mathbf{Q}$ at time t, if it was in $\mathbf{Q}_0$ at some previous time t_0; $\hat{\mathbf{M}}(\boldsymbol{\Omega})$ is the infinitesimal rotation operator, $\partial/\partial\boldsymbol{\theta}$ the gradient on the torsion angles. $\mathbf{D}_{RR}$, $\mathbf{D}_{II}$, and $\mathbf{D}_{RI}$ are, respectively, the pure rotational, pure configurational, and roto-configurational parts of the 7×7 diffusion tensor $\mathbf{D}(\mathbf{Q})$. Finally, $P_{eq}(\mathbf{Q})$ is the Boltzmann equilibrium probability distribution

$$P_{eq}(\mathbf{Q}) = \exp\left[-A(\mathbf{Q})/k_BT\right]/\left\langle\exp\left[-A(\mathbf{Q})/k_BT\right]\right\rangle \qquad (2)$$

where k_B is the Boltzmann constant, T the absolute temperature, and $A(\mathbf{Q})$ the potential of mean force acting on $\mathbf{Q}$. The potential of mean force $A(\mathbf{Q})$ was inferred from the analysis of molecular dynamics (MD) simulations (see below).

Solution of eq 1 is usually carried out by spanning the diffusive operator $\hat{\Gamma}(\mathbf{Q})$ over a proper basis set and solving the corresponding eigensystem. In this case, however, since the number of coordinates is 7 (3 rotational + 4 internal), the dimensionality of the matrix is expected to be prohibitive in terms of memory and computation time. Thus, we decided to follow a second route, viz., solving numerically the Langevin equation associated to eq 1. To this end, we employed the BD_BOX software package.[24] It is programmed to evolve the Brownian dynamics (BD) of a set of beads (atoms or extended atoms) in Cartesian coordinates

$$\dot{\mathbf{x}} = -\mathbf{D}(\mathbf{x})\frac{\partial A(\mathbf{x})}{\partial\mathbf{x}} + \left[2\mathbf{D}(\mathbf{x})\right]^{1/2}\boldsymbol{\eta}(t) \qquad (3)$$

where $\mathbf{x}$ is the set of Cartesian coordinates of the beads, $\mathbf{D}(\mathbf{x}) = \mathbf{D}\left[\mathbf{Q}(\mathbf{x})\right]$ is the (configuration dependent) diffusion tensor, $A(\mathbf{x})$ is the potential of mean force, and $\boldsymbol{\eta}(t)$ is the array of white noise source on each variable.

Eq 3 is lacking the term $\left[\partial\mathbf{D}(\mathbf{x})/\partial\mathbf{x}\right]^{tr}$, not implemented in BD_BOX, which is a contribution originated from the gradient of the diffusion tensor. Nevertheless, for small molecules, it can be

expected to be small compared to the other two terms appearing in eq 3, since a change in the torsion angles does not drastically affect the overall molecular shape. To give a semi-qualitative justification to such an assertion, the configuration-dependent diffusion tensor has been evaluated also with an independent computational tool, via an extended hydrodynamics approach, implemented in the DiTe software.[25] In the case of GGM, the roto-conformational diffusion tensor is represented by a 7×7 matrix partitioned as shown in eq 1.

Potential of mean force. The potential of mean force (which is in effect a Helmholtz free energy), could be accessed by means of different molecular dynamics (MD) simulations approaches. The most effective are biased MD calculations, which allow a better/faster sampling of the Boltzmann equilibrium distribution (with the counter effect that kinetics of the exploration of the potential surface is 'artificial').[26] From past work on oligosaccharides knowledge has emerged that the free energy surface can be approximated as a sum of two-dimensional surfaces of the (ϕ,ψ) couples as

$$A(\boldsymbol{\theta}) \approx \sum_{i=1}^{N} A_i(\phi_i,\psi_i) \tag{4}$$

where N is the number of sugar linkages and the shape of $A_i(\phi,\psi)$ depends on the specific i-th linkage type.

Moreover, a recent study[11] on bi-dimensional torsional free energy profiles of trisaccharides in which the sugar units are conjoined by different linkage types, showed that the shape of $A_i(\phi,\psi)$ mostly depend on the configuration of the linkage. Taking as reference the work on five trisaccharides by Yang et al.[11] the shapes of $A_i(\phi,\psi)$ for α-linked residues are all very similar. By the same token, the glycosidic free energy surfaces for β-linked residues are indeed quite similar. Thus, tentatively, these MD simulation results can be seen as a parametrization of a Brownian dynamics force field for oligosaccharides. Thus, we shall parametrize the potential of mean force in the case of GGM (which is molecule **3** in the study by Yang et al.[11]) as

$$A(\boldsymbol{\theta}) \approx A_\beta(\phi_2,\psi_2) + A_\beta(\phi_3,\psi_3) \tag{5}$$

Herein, a further approximation is carried out since BD_BOX does not implement 2D potential surfaces. We split each of the two terms appearing in eq 5 as $A_\beta(\phi,\psi) \approx A_\beta(\phi) + A_\beta(\psi)$ where

$$A_\beta(\phi) = C(T) - k_B T \int_0^{2\pi} d\psi e^{-A_\beta(\phi,\psi)/k_B T} \tag{6}$$

and an analogous expression holds for $A_\beta(\psi)$. The four integrals have been carried out numerically from the discretized representation of the $A_\beta(\phi,\psi)$ free energy surfaces taken from the work by Yang et al.[11] The goodness of such an approximation must be validated a posteriori, from the agreement of the calculated NMR data with the experimental ones.

Results and Discussion

NMR spin relaxation experiments. To obtain dynamical information from NMR spin relaxation experiments of small molecules such as disaccharides the use of solvents or solvent mixtures that have a higher viscosity than water greatly facilitates acquisition of data outside the extreme narrowing region. For disaccharides we have previously used DMSO-d_6,[27] and the cryo-solvent D_2O:DMSO-d_6 in a 7:3 ratio,[28] which has also been employed for trisaccharides.[29] In D_2O as a solvent at 298 K the trisaccharide GGM shows a heteronuclear NOE factor, 2.27 – 2.47, well below the theoretical maximum of 2.99, at the two magnetic field strengths, viz., 14.1 T and 16.4 T, employed in this study (Table 1). Subsequently, ^{13}C NMR spin-lattice relaxation times T_1 and spin-spin relaxation times T_2 were acquired. For the GGM trisaccharide dual very high ^{13}C-labeling of 99 atom% at the C2'- and C2''-positions was available,[11] referred to as [$^{13}C_2$]-GGM, which facilitates a comparative study using the exactly same experimental conditions for the two ^{13}C-spins. The quality of the acquired NMR spin relaxation data for [$^{13}C_2$]-GGM was very high and the standard deviation for all NMR relaxation data was ≤ 0.5% (Table 1).

Table 1. Experimental and calculated ^{13}C NMR relaxation data for the trisaccharide [$^{13}C_2$]-GGM in D_2O at 298.6 K.

	^{1}H frequency /MHz	Experimental[a]		Calculated		%Error	
		C2''	C2'	C2''	C2'	C2''	C2'
T_1 /ms	600.13	491.6	456.2	483.5	454.9	-1.6	-0.3
T_2 /ms		450.2	416.6	456.8	421.1	+1.5	+1.1
NOE		2.466	2.398	2.529	2.437	+2.6	+1.6
T_1 /ms	699.87	524.5	491.1	520.8	493.9	-0.7	+0.6
T_2 /ms		483.9	447.4	486.8	450.0	+0.6	+0.6
NOE		2.346	2.267	2.414	2.319	+2.9	+2.3

[a] Standard deviations for T_1, T_2 and NOE are ≤ 0.1%, ≤ 0.5% and ≤ 0.5%, respectively.

Brownian dynamics simulations. Since the diffusion tensor of GGM is represented by a 7×7 matrix partitioned as shown in eq 1 (vide infra) we plot selected coefficients of the diffusion tensor as functions of the molecular geometry, evaluated in water at 298.6 K. In particular, the coefficients shown are the isotropic part of the rotational diffusion tensor (Figure 2), and the four diagonal values of the configurational block of the diffusion tensor (Figure 3); panels on the left show the dependence on (ϕ_2,ψ_2) while the other two torsion angles are fixed at the lowest energy configuration. Analogously, panels on the right display the dependence upon (ϕ_3,ψ_3). Contour plots delimiting regions where the potential of mean force is below than 5 k_BT are superposed to show that in the most representative configurations of the molecule the diffusion tensor coefficients change is only 5 – 10%. Such a small dependence justifies neglecting the contribution to the velocity of the beads originated from the gradient of the diffusion tensor.

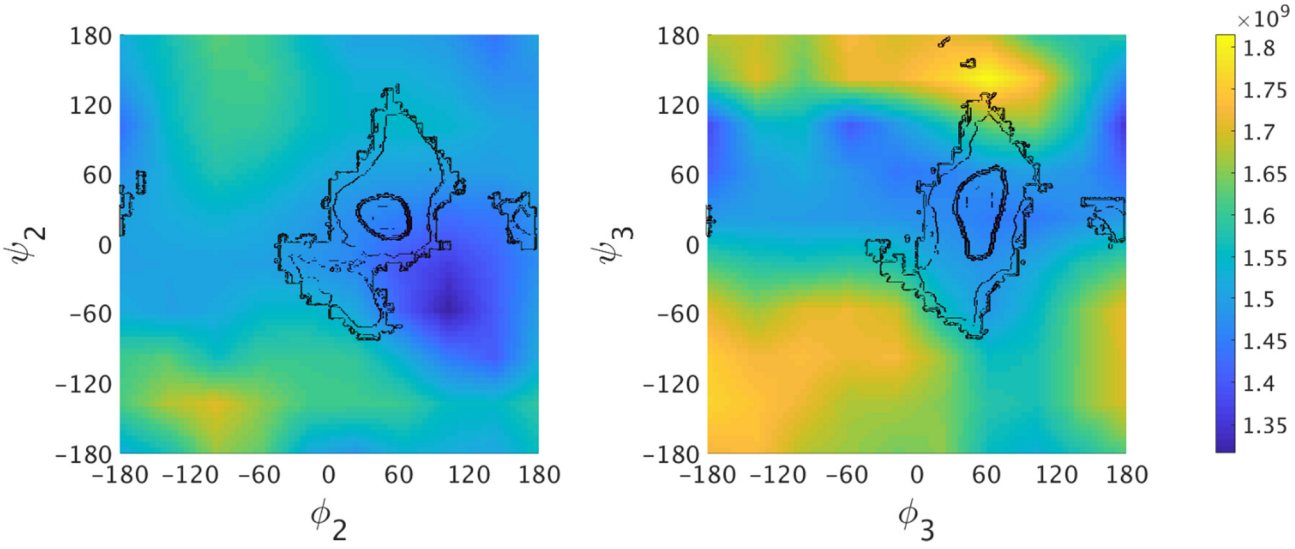

Figure 2. Dependence of isotropic part of the rotational block of the diffusion tensor on the (ϕ_2,ψ_2) couple (left panel), and the (ϕ_3,ψ_3) couple (right panel) of torsion angles. Values of the diffusion coefficient are given in color code; units are Hz. The black contour plots show the regions where the potential of mean force is below 5 k_BT.

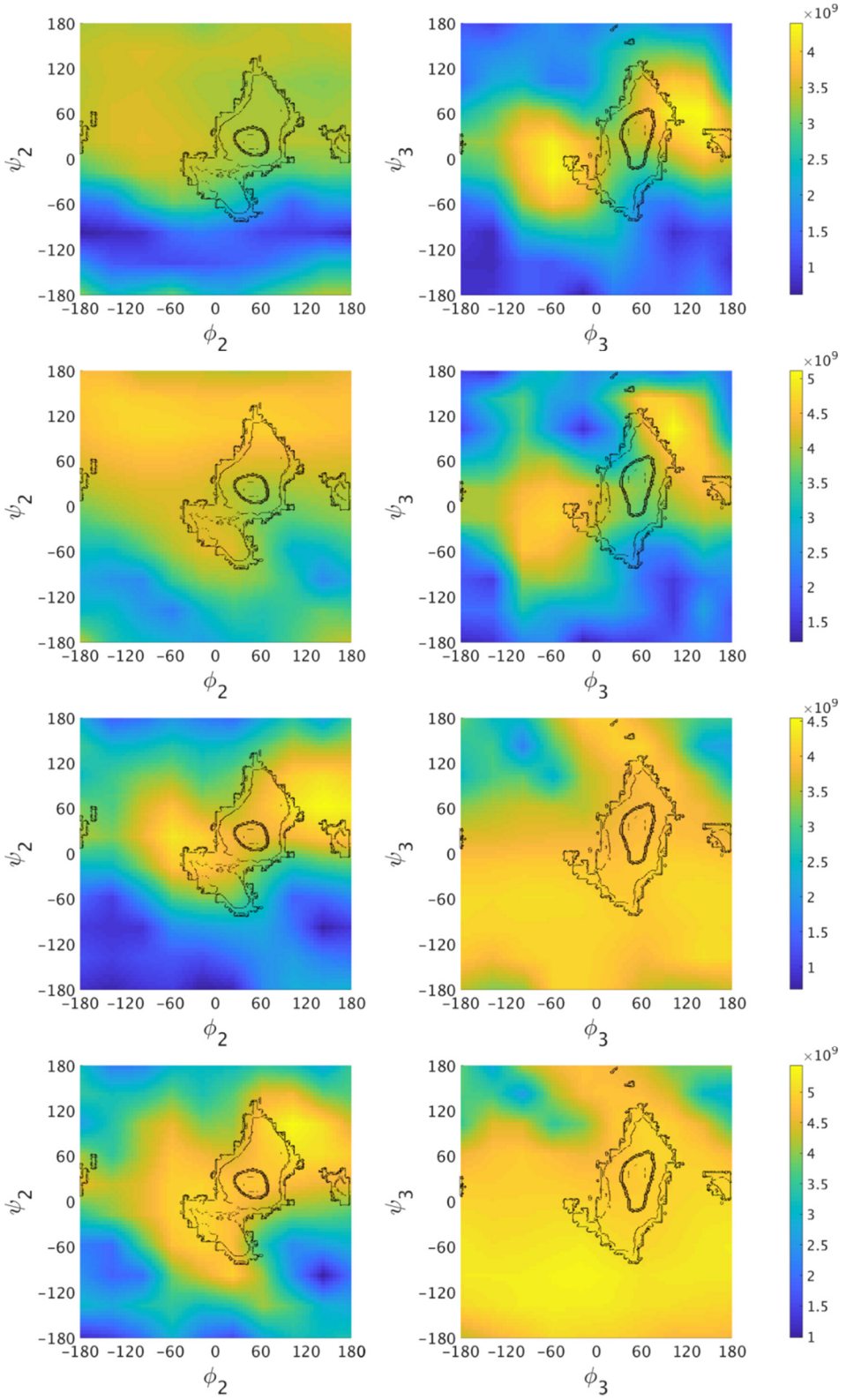

Figure 3. Dependence of $\left(\mathbf{D}_{II}\right)_{j,j}$, with j from 1 (top) to 4 (bottom), configurational diffusion coefficients on the $\left(\phi_2,\psi_2\right)$ couple (panels on the left), the $\left(\phi_3,\psi_3\right)$ couple (panels on the right) of torsion angles. Values of the diffusion coefficients are given in color code; units are Hz. The black contour plots show the regions where the potential of mean force is below 5 k_BT.

Given the complex shape of the free energy profiles (Figure 4), which are difficult to represent by means of usual cosine functions available for MD simulations, the BD_BOX software package has been modified in order to calculate the force from a torsional potential expressed as a truncated combination of complex exponentials

$$A(\theta) = \sum_{n=-N}^{N} a_n e^{-in\theta} \tag{7}$$

The four one-dimensional torsion angle potential of mean force profiles have been fitted with the above expansion and parameters are reported in Table 2.

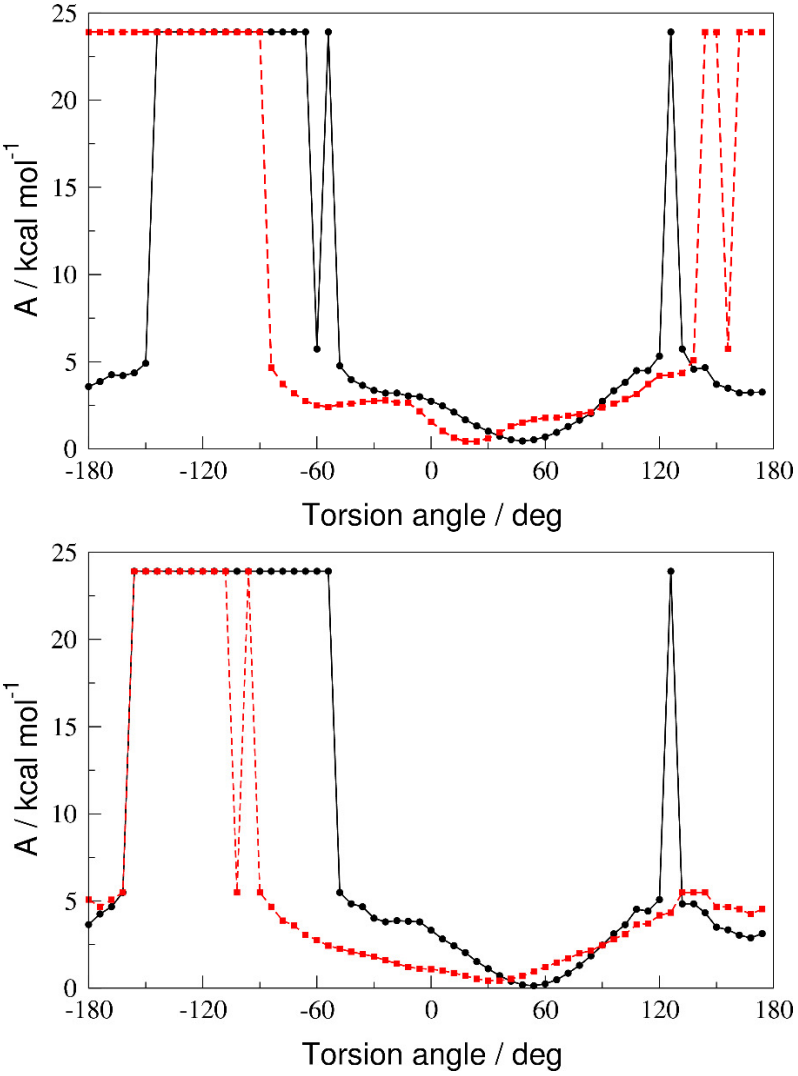

Figure 4. One-dimensional free energy profiles for the ϕ_2 and ψ_2 torsion angles (top panel) and the ϕ_3 and ψ_3 torsion angles (bottom panel). $A(\phi)$ is represented with black filled circles and a solid line, while $A(\psi)$ with red filled squares and a dashed line.

Table 2. Coefficients of the expansion of the four one-dimensional torsional angle free energy profiles over the basis of complex exponentials (eq 7). All coefficients are given in kcal·mol^{-1} and only for $n \geq 0$ since the $a_{-n} = a_n^*$ constraint holds for the potential to be real.

Coefficient	$A(\phi_2)$	$A(\psi_2)$	$A(\phi_3)$	$A(\psi_3)$
a_0	4.870	15.96	15.84	3.734
a_1	-0.8367-1.856i	-10.40-7.618i	-3.653-11.91i	-1.437-0.9058i
a_2	-1.079+0.02009i	2.719+9.296i	-8.397+4.801i	-0.2398+0.4063i
a_3	0.86320+0.5770i	2.557-6.599i	6.074+4.965i	0.4934-0.1287i
a_4	0.1500-0.2935i	-3.555+2.221i	2.133-4.540i	-0.2240-0.1407i
a_5	-0.2336-0.07829i	2.192-0.1321i	-3.104-0.5392i	0.05789+0.09841i
a_6	0.09436+0.2346i	-0.7055-0.4703i	0.2424+1.755i	0.02400+0.002847i
a_7	0.05857-0.1005i	0.1319+0.1614i	0.7121-0.3492i	-0.0004607+0.001173i
a_8	0	0	-0.1498-0.1667i	-0.01807+0.02297i

The remaining internal degrees of freedom should be kept fixed at their energy minimum value. Such a constraint is not implemented in BD_BOX; thus, we modeled the non-essential internal degrees of freedom as subjected to harmonic potentials with hard force constants. In particular, the force constants for bond lengths, angles and torsion angles were set to 2000 kcal·mol^{-1}·Å^2, 200 kcal·mol^{-1}, and 20 kcal·mol^{-1}, respectively. Using such tight potential force constants, the integration time step needed to be set to 1 fs. In our simulations, the beads were uncharged (no electrostatic interactions). Temperature was set at 298.6 K and viscosity of D_2O to $1.09 \cdot 10^{-2}$ Pa·s. Dynamics of GGM was simulated in an unlimited, non-periodic box.

Initially, a 20 ns long trajectory was produced; from it 50 configurations were randomly drawn and used as starting configurations for 50 production trajectories of duration 20 ns each (thus, a total of 1 μs), saving a configuration of the GGM molecule each 0.5 ps. Initial velocities were re-initialized for each of the 50 runs using a different seed for the pseudo-random numbers generator. To speed up simulations we evolved the trajectory of heavy atoms only, setting a 2 Å radius for the calculation of the diffusion tensor, a procedure usually followed in the hydrodynamic calculation of diffusion tensors.[25] Six hydrogen atoms were explicitly included in the simulations. Four of them, in particular H1', H2, H1", and H3 (see Figure 1) were needed to define the torsion angles, which we recall are

defined as ϕ_2 = H1'-C1'-O2-C2, ψ_2 = C1'-O2-C2-H2, ϕ_3 = H1"-C1"-O3-C3, ψ_3 = C1"-O3-C3-H3. The other two hydrogen atoms were those attached to the two ^{13}C atoms for which NMR data has been experimentally measured, i.e. H2' and H2". While not strictly necessary, we kept the latter two H atoms to simplify the post-run analysis of the BD simulations.

From each of the trajectories the time series of the spherical angles β for the two NMR probes have been extracted, which are the angles between the ^{13}C-^{1}H bonds and the Z-axis of the LF. Subsequently, the time series for the $D^2_{0,0}(\beta)$ Wigner matrices were calculated. Finally, their autocorrelation functions were extracted. For each of the NMR probes, the average over the 50 autocorrelation functions has been carried out. The resulting correlation function has been shifted to have no plateau (a small plateau was observed due to very bad rotational exploration of some trajectories), the first point removed, time shifted and finally normalized. The removal of the first point is usually done since it counts very fast, nearly decoupled, motions due to relaxation of momenta which are not part of the DCM model. Even if the number of trajectories is high and protracted for at least 100 times longer than the correlation time, the autocorrelation functions, as shown in Figure 5, are still too noisy in their tails to be used to produce usable spectral densities. Thus, we decided to smooth the data by fitting the BD-derived autocorrelation functions with the functional form

$$C(t) = A^2 e^{(-t/\tau_A)^\alpha} + (1 - A^2) e^{(-t/\tau_B)^\beta} \qquad (8)$$

We shall stress here that eq 8 has been selected exclusively for its adaptability to fit satisfactorily the autocorrelation functions. These are in general an infinite sum of exponential decays and there is no physical reason, within a Markovian description of relevant coordinates, in the parameters of a bi-stretched exponential form. Parameters for the two probes are the following: for C2', $A = 0.902956$, $\tau_A = 0.195764$ ns, $\alpha = 1.05611$, $\tau_B = 82.21686$ ps, and $\beta = 0.469077$; for C2", instead, $A = 0.96344$, $\tau_A = 0.173916$ ns, $\alpha = 1.01493$, $\tau_B = 4.68923$ ps, and $\beta = 0.508517$. A separation between a sub-ns and a ns time scales is observed. The faster time scale is associated to the fast librations of the non-relevant degrees of freedom (not rigid in our BD simulations). However, the weight of such a relaxation process is very small compared with the slower one. The two probes show a small, rather important, difference on the ns-scale correlation time.

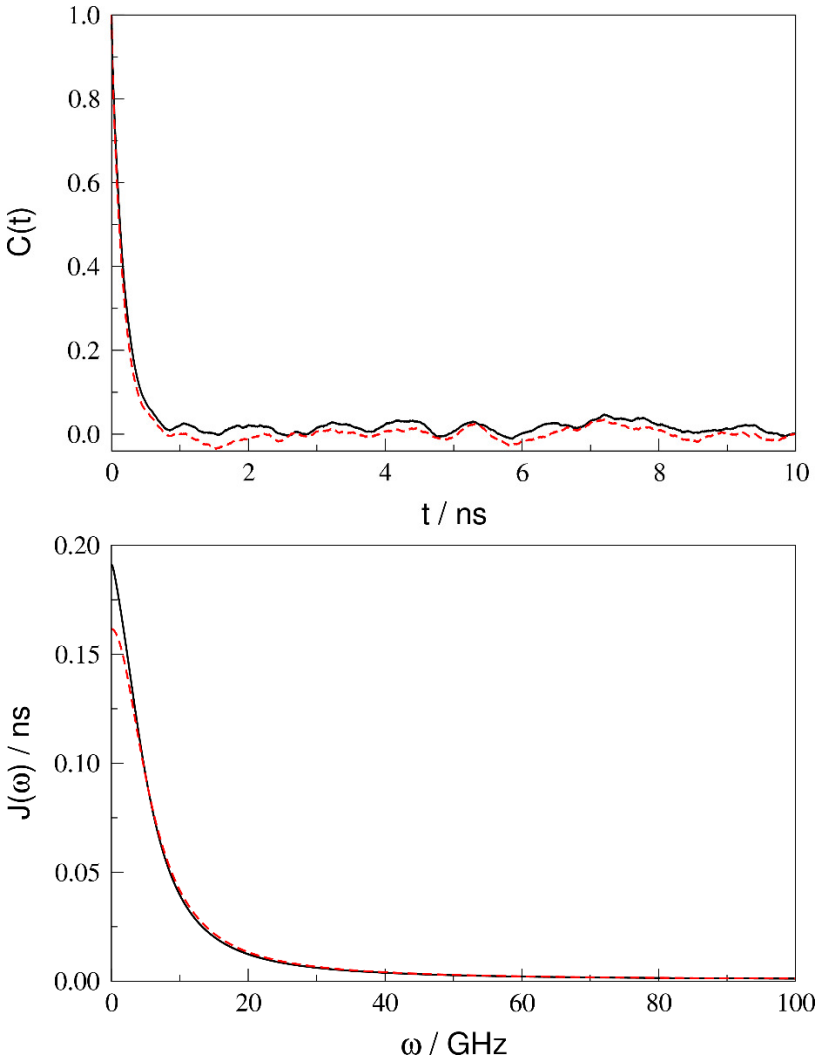

Figure 5. Autocorrelation functions (top panel) and spectral densities (bottom panel) for the $D^2_{0,0}(\beta)$ function of C2' (black, solid line) and C2" (red, dashed line) probes. Note the difference at $J(0)$, where for the former $\tau_A = 0.196$ ns and for the latter $\tau_A = 0.174$ ns.

From the smoothed autocorrelation functions the corresponding spectral densities have been calculated (Figure 5) and employed in the computation of NMR relaxation data using standard relations.[30] For the ^{13}C-^{1}H probe we set $\delta_{CSA} = 0$ and the bond length $r_{CH} = 1.13$ Å, longer with respect to the C-H bond length in order to take into account for the vibrational corrections.[31,32] Comparison with experiments is provided in Table 1. The agreement with experimental data is indeed quite satisfactory, where deviations are < 3% in all cases of acquired NMR relaxation parameters, even if a number of approximations were applied. We would like to stress that the computational protocol was applied without fitting of any parameters, like in recent NMR studies of oligosaccharide dynamics, such as the pentasaccharide LNF-1[33] where NMR data was acquired for ^{13}C at natural abundance and the disaccharide α-L-[1'-^{13}C]Rha*p*-(1→2)-α-L-Rha*p*-OMe[17] site-selectively ^{13}C-labeled to 99 atom-%.[34]

Conclusions

In this work, we investigated the dynamics of the two types of linkages between glucosyl residues under identical experimental conditions. The high quality of the acquired NMR spin relaxation data allows us to distinguish between the different local dynamics of the two glycosidic linkages. Since all the details of the structure and dynamics of the molecule are affecting the experimental data in a non-trivial manner, a comprehensive model is required to rationalize the different linkages' dynamical behaviors. The analysis based on the DCM was shown to be an effective approach to interpret NMR relaxation data. The oligosaccharide internal energy is represented as the potential of mean force (POMF) given by a sum of couples of dihedral angles (ϕ,ψ) terms, and the dynamics of all the dihedrals is described by a diffusive model governed by a diffusion tensor. Different couples of dihedral angles interact only hydrodynamically. Moreover, since the POMF surfaces show only one pronounced minimum (with other relative minima at higher energy and separated by large barriers > 5 k_BT), the diffusion tensor can be safely assumed to be constant, i.e. independent from the molecular geometry. The protocol is summarized as follows: (*i*) the non-dihedral internal degrees of freedom are considered a priori as fast; (*ii*) short MD simulations are used to access dihedral angles correlation functions, which are employed to identify the relevant torsion angles as those showing slow decays (compatible with NMR relaxation); (*iii*) MD simulations are employed to access the potential of mean force over the relevant torsion angles; (*iv*) long (μs time scale) Brownian dynamics simulations in internal coordinates give direct access to the correlation functions and spectral densities used to calculate NMR relaxation parameters. We would like to comment further on points (*iii*) and (*iv*) to suggest future strategies to make the DCM approach even more effective to interpret NMR relaxation data in small/medium flexible molecules. First of all, here and previously,[15,16,17] it has been shown that for oligosaccharides the POMF of the (ϕ,ψ) couples of dihedrals in different types of linkages is broadly molecule-independent. It would be reasonable in many cases to consider the POMF surfaces calculated for different types of linkages as independent on the specific molecular system,[9] thereby omitting the MD simulation step (*iii*) of the protocol described above. Next it should be convenient to implement a BD computational approach working out the dynamics directly in internal, instead of Cartesian coordinates. Although slightly more cumbersome from the technical point of view, such an approach should present a number of benefits, like the reduced dimensionality of the resulting trajectories, the possibility of using a larger time step and the avoidance of spurious fast components in the spectral densities.

Acknowledgements

This work was supported by grants from the Swedish Research Council (no. 2013-4859), The Knut and Alice Wallenberg Foundation, "Fondazione della Cassa di Risparmio di Padova e Rovigo" (CARIPARO), project M3PC, and by the University of Padua (P-DISC #CARL-SID17 BIRD2017-UNIPD), project CHIRoN. All simulations have been run on the C3P ("Computational Chemistry Community in Padua") HPC facility of the Department of Chemical Sciences of the University of Padua.

References

(1) Mariño, K.; Bones, J.; Kattla, J. J.; Rudd, P. M. A Systematic Approach to Protein Glycosylation Analysis: A Path through the Maze. *Nat. Chem. Biol.* **2010**, *6*, 713–723.

(2) Krishnan, V. V.; Rupp, B. Macromolecular Structure Determination: Comparison of X-Ray Crystallography and NMR Spectroscopy. In *eLS*; John Wiley & Sons, Ltd: Chichester, UK, 2012; pp 1–13.

(3) Murata, K.; Wolf, M. Cryo-Electron Microscopy for Structural Analysis of Dynamic Biological Macromolecules. *Biochim. Biophys. Acta - Gen. Subj.* **2017**, *1862*, 324–334.

(4) Weinreis, S. A.; Ellis, J. P.; Cavagnero, S. Dynamic Fluorescence Depolarization: A Powerful Tool to Explore Protein Folding on the Ribosome. *Methods* **2010**, *52*, 57–73.

(5) Palmer III, A. G. NMR Probes of Molecular Dynamics: Overview and Comparison with Other Techniques. *Annu. Rev. Biophys. Biomol. Struct.* **2001**, *30*, 129–155.

(6) Vliegenthart, J. F. G. The Impact of Defining Glycan Structures. *Perspect. Sci.* **2017**, *11*, 3–10.

(7) Widmalm, G. A Perspective on the Primary and Three-Dimensional Structures of Carbohydrates. *Carbohydr. Res.* **2013**, *378*, 123–132.

(8) Dalheim, M.; Arnfinnsdottir, N. B.; Widmalm, G.; Christensen, B. E. The Size and Shape of Three Water-Soluble, Non-Ionic Polysaccharides Produced by Lactic Acid Bacteria: A Comparative Study. *Carbohydr. Polym.* **2016**, *142*, 91–97.

(9) Turupcu, A.; Oostenbrink, C. Modeling of Oligosaccharides within Glycoproteins from Free-Energy Landscapes. *J. Chem. Inf. Model.* **2017**, *57*, 2222–2236.

(10) Frank, M.; Collins, P. M.; Peak, I. R.; Grice, I. D.; Wilson, J. C. An Unusual Carbohydrate Conformation Is Evident in Moraxella Catarrhalis Oligosaccharides. *Molecules* **2015**, *20*, 14234–14253.

(11) Yang, M.; Angles d'Ortoli, T.; Säwén, E.; Jana, M.; Widmalm, G.; MacKerell Jr, A. D. Delineating the Conformational Flexibility of Trisaccharides from NMR Spectroscopy Experiments and Computer Simulations. *Phys. Chem. Chem. Phys.* **2016**, *18*, 18776–18794.

(12) Kjellberg, A.; Widmalm, G. A Conformational Study of the Vicinally Branched

Trisaccharide β-D-Glcp-(1→2)[β-D-Glcp-(1→3)]α-D-Manp-OMe by Nuclear Overhauser Effect Spectroscopy (NOESY) and Transverse Rotating-Frame Overhauser Effect Spectroscopy (TROESY) Experiments: Comparison. *Biopolymers* **1999**, *50*, 319–399.

(13) Kjellberg, A.; Rundlöf, T.; Kowalewski, J.; Widmalm, G. Motional Properties of Two Vicinally Disubstituted Trisaccharides as Studied by Multiple-Field Carbon-13 NMR Relaxation. *J. Phys. Chem. B* **1998**, *102*, 1013–1020.

(14) Zerbetto, M.; Polimeno, A. Multiscale Modeling for Interpreting Nuclear Magnetic Resonance Relaxation in Flexible Molecules. *Int. J. Quantum Chem.* **2016**, *116*, 1706–1722.

(15) Kotsyubynskyy, D.; Zerbetto, M.; Soltesova, M.; Engström, O.; Pendrill, R.; Kowalewski, J.; Widmalm, G.; Polimeno, A. Stochastic Modeling of Flexible Biomolecules Applied to Nmr Relaxation. 2. Interpretation of Complex Dynamics in Linear Oligosaccharides. *J. Phys. Chem. B* **2012**, *116*, 14541–14555.

(16) Zerbetto, M.; Polimeno, A.; Kotsyubynskyy, D.; Ghalebani, L.; Kowalewski, J.; Meirovitch, E.; Olsson, U.; Widmalm, G. An Integrated Approach to NMR Spin Relaxation in Flexible Biomolecules: Application to β-D-Glucopyranosyl-(1→6)-α-D-Mannopyranosyl-OMe. *J. Chem. Phys.* **2009**, *131*, 234501.

(17) Pendrill, R.; Engström, O.; Volpato, A.; Zerbetto, M.; Polimeno, A.; Widmalm, G. Flexibility at a Glycosidic Linkage Revealed by Molecular Dynamics, Stochastic Modeling, and 13C NMR Spin Relaxation: Conformational Preferences of α-L-Rhap-(1→2)-α-L-Rhap-OMe in Water and Dimethyl Sulfoxide Solutions. *Phys. Chem. Chem. Phys.* **2016**, *18*, 3086–3096.

(18) Hermosilla, L.; Sieiro, C.; Calle, P.; Zerbetto, M.; Polimeno, A. Modeling of Cw-EPR Spectra of Propagating Radicals in Methacrylic Polymerization at Different Temperatures. *J. Phys. Chem. B* **2008**, *112*, 11202–11208.

(19) Zerbetto, M.; Polimeno, A.; Cimino, P.; Barone, V. On the Interpretation of Continuous Wave Electron Spin Resonance Spectra of Tempo-Palmitate in 5-Cyanobiphenyl. *J. Chem. Phys.* **2008**, *128*, 024501.

(20) Jansson, P.-E.; Kjellberg, A.; Rundlöf, T.; Widmalm, G. Synthesis, NMR Spectroscopy and Conformational Studies of Two Vicinally Disubstituted Trisaccharides. *J. Chem. Soc. Perkin Trans. 2* **1996**, 33–37.

(21) Findeisen, M.; Brand, T.; Berger, S. A 1H-NMR Thermometer Suitable for Cryoprobes. *Magn. Reson. Chem.* **2007**, *45*, 175–178.

(22) Canet, D.; Levy, G. C.; Peat, I. R. Time Saving in 13C Spin-Lattice Relaxation Measurements by Inversion-Recovery. *J. Magn. Reson.* **1975**, *18*, 199–204.

(23) Meiboom, S.; Gill, D. Modified Spin-Echo Method for Measuring Nuclear Relaxation Times. *Rev. Sci. Instrum.* **1958**, *29*, 688–691.

(24) Dlugosz, M.; Zielinski, P.; Trylska, J. Brownian Dynamics Simulations on CPU and GPU with BD_BOX. *J. Comput. Chem.* **2011**, *32*, 2734–2744.

(25) Barone, V.; Zerbetto, M.; Polimeno, A. Hydrodynamic Modeling of Diffusion Tensor Properties of Flexible Molecules. *J. Comput. Chem.* **2009**, *30*, 2–13.

(26) *Free Energy Calculations. Theory and Applications in Chemistry and Biology*; Chipot, C., Pohorille, A., Eds.; Springer Verlag: Berlin, 2007.

(27) Söderman, P.; Widmalm, G. Conformational Flexibility of Disaccharides Investigated by Multiple Field Carbon-13 Nuclear Spin Relaxation. *Magn. Reson. Chem.* **1999**, *37*, 586–590.

(28) Mäler, L.; Widmalm, G.; Kowalewski, J. Dynamical Behavior of Carbohydrates as Studied by Carbon-13 and Proton Nuclear Spin Relaxation. *J. Phys. Chem.* **1996**, *100*, 17103–17110.

(29) Mäler, L.; Lang, J.; Widmalm, G.; Kowalewski, J. Multiple-Field Carbon-13 NMR Relaxation Investigation on Melezitose. *Magn. Reson. Chem.* **1995**, *33*, 541–548.

(30) Abragam, A. *The Principles of Nuclear Magnetism*; Claredon Press: Oxford, U.K., 1961.

(31) Henry, E. R.; Szabo, A. Influence of Vibrational Motion on Solid State Line Shapes and NMR Relaxation. *J. Chem. Phys.* **1985**, *82*, 4753–4761.

(32) Kowalewski, J.; Effemey, M.; Jokisaari, J. Dipole-Dipole Coupling Constant for a Directly Bonded CH Pair--a Carbon-13 Relaxation Study. *J. Magn. Reson.* **2002**, *157*, 171–177.

(33) Rundlöf, T.; Venable, R. M.; Pastor, R. W.; Kowalewski, J.; Widmalm, G. Distinguishing Anisotropy and Flexibility of the Pentasaccharide LNF-1 in Solution by Carbon-13 NMR Relaxation and Hydrodynamic Modeling. *J. Am. Chem. Soc.* **1999**, *121*, 11847–11854.

(34) Jonsson, K. H. M.; Säwén, E.; Widmalm, G. Studies on the Conformational Flexibility of α-L-Rhamnose-Containing Oligosaccharides Using 13C-Site-Specific Labeling, NMR Spectroscopy and Molecular Simulations: Implications for the Three-Dimensional Structure of Bacterial Rhamnan Polysaccharides. *Org. Biomol. Chem.* **2012**, *10*, 2453–2463.

TOC Graphic

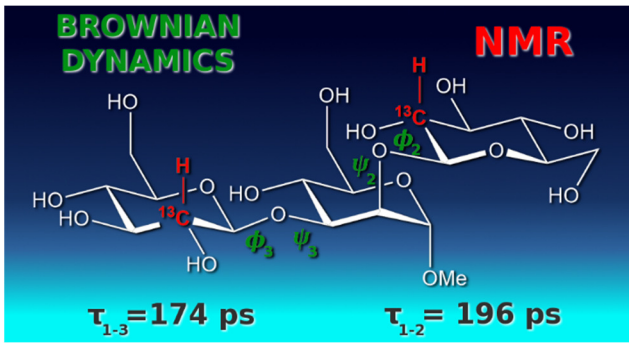
BROWNIAN
DYNAMICS
NMR
HO
OH
H
13C
OH
HO
Φ2
O
O
OH
Ψ2
HO
HO
H
O
HO
O
13C
O
HO
Φ3
Ψ3
OMe
τ1-3=174 ps
τ1-2= 196 ps